Steel and Composite Structures, Vol. 13, No. 3 (2012) 259-275
DOI: http://dx.doi.org/10.12989/scs.2012.13.3.259

Parametric study on bearing capacity of CFST members considering the concrete horizontal casting effect

Wenbo Sun*[1], Yiqun Luo[2], Weijian Zhou[2], and Wei Huang[3]

[1]*Architect Design and Research Institute, South China University of Technology, Guangzhou, P.R.China*
[2]*School of Civil and Traffic Engineering, South China University of Technology, Guangzhou, P.R.China*
[3]*School of Science and Engineering, Jinan University, Guangzhou, P.R.China*

(Received April 17, 2011, Revised May 09, 2012, Accepted May 30, 2012)

Abstract. Concrete filled steel tubular (CFST) member has been widely used in the construction of high-rise buildings for its high axial bearing capacity. It can also be applied on long-span structures such as spatial structures or bridges not only for its high bearing capacity but also for its construction convenience. Concrete casting effect of CFST member is considered in the study of its bearing capacity in this paper. Firstly, in order to authenticate the applicability of constitutive relationship and yield criterion of steel and concrete based on FEM, two ANSYS models are built to simulate and compared with other's test. Secondly, in order to find the huge difference in bearing capacity due to different construction processes, two full-size CFST models are studied when they are horizontally cast and axially compressed. Finally, the effects of slenderness ratio (L/D) and confining parameter (D/t) of CFST members are studied to reveal the intrinsic links between bearing capacity and slenderness ratio or confining parameter.

Keywords: CFST; bearing capacity; the nonlinear finite element method; concrete horizontal casting effect.

1. Introduction

Concrete filled steel tubular (CFST) member, a kind of composite element of steel tube filled with concrete, possesses great compressive capacity for the interaction between steel tube and core concrete. In addition to its high compressive strength, CFST member has other great mechanical properties such as good ductility, relatively small size, high performance on fire resistance and high construction efficiency, etc (e.g., Han 2007).

Recent researches about initial stress of CFST have mainly concentrated in its effect on bearing capacity of the vertically placed members (e.g., Furlong 1967). However, there are usually some horizontal CFST members in long-span structures such as bridges and trusses. Meanwhile, in order to reduce temporary supports used for the horizontal construction of CFST, a simple but reasonable method is to cast concrete into simply-supported and horizontally-placed steel tube directly. A typical application of this method is on the construction of Century Lotus Stadium in Foshan Sport Center (Fig. 1), whose roof is a wheel-spoke cable-membrane structure with 155 m-radius upper compress ring and 138 m-radius lower compress ring. Because of the huge axial compression in these two rings,

* Corresponding author, Ph.D., E-mail: sunwenbo@scut.edu.cn

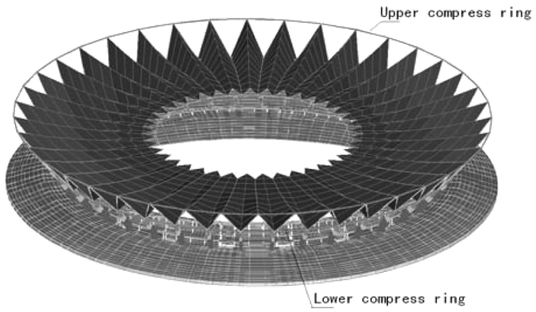

Fig. 1 Foshan Century Lotus Stadium

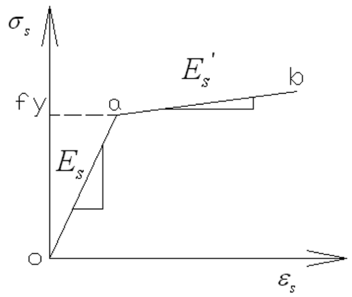

Fig. 2 the stress-strain relation of steel

horizontal casting CFST member is valuable for the reduction of construction cost.

Casting concrete into a horizontally-placed and simply-supported steel tube will inevitably produce initial stress in tubes and cause initial deflection in the middle of CFST members before concrete setting and hardening. The phenomenon is named as “concrete horizontal casting effect” in this paper. It is necessary to study this effect on the bearing capacity of horizontally cast CFST members at all stages. In this paper, finite element software ANSYS is used to simulate the concrete casting effect on the axial bearing capacity of the horizontally cast CFST members.

2. Constitutive relationships of steel and concrete

2.1 Constitutive relationship of steel

Constitutive relationship of steel consists of elastic and elastic-plastic stages shown in Fig. 2.

Elastic stage (o-a) [$\sigma_i \le f_y$]. At this stage, the stress-strain relation of steel is linear, which can be written as incremental equation as Eq. (1) (e.g., Han 2007)

$$d\{\sigma\} = d\begin{Bmatrix}\sigma_1\\ \sigma_2\\ \sigma_3\end{Bmatrix} = [D]_e d\begin{Bmatrix}\varepsilon_1\\ \varepsilon_2\\ \varepsilon_3\end{Bmatrix} \tag{1}$$

Elastic-plastic strengthening stage (a-b) [$f_y \le \sigma_i$]. Use Linear Kinematic Hardening Model (e.g., Zha and Zhong 1997) as Eq. (2)

$$\begin{aligned} d\sigma_{ij} &= [D]_{ep} d\varepsilon_{ij} \\ [D]_{ep} &= [D]_e - [D]_p \end{aligned} \tag{2}$$

Where E_s in Fig.2 is the Young's modulus of steel, where

$$E'_s = 0.005 E_s$$

2.2 Constitutive relationship of concrete

The constitutive relationship of core concrete is presented by Han (2007), Attard (1996) and Lubliner (1996). The stress-strain relationship can be written as Eq. (3a) and Eq. (3b)

$$y = 2x - x^2 \qquad (x \le 1) \tag{3a}$$

$$y = \begin{cases} 1 + q(x^{0.1\xi} - 1) & (\xi \ge 1.12) \\ \dfrac{x}{\beta(x-1)^2 + x} & (\xi < 1.12) \end{cases} \qquad (x > 1) \tag{3b}$$

Where: $x = \dfrac{\varepsilon}{\varepsilon_o}$; $y = \dfrac{\sigma}{\sigma_o}$

$$\sigma_o = \left[1 + (-0.054\xi^2 + 0.4\xi)\left(\frac{24}{f_c}\right)^{0.45}\right] f_c$$

$$\varepsilon_o = \varepsilon_{cc} + \left[1400 + 800\left(\frac{f_c}{24} - 1\right)\right]\xi^{0.2} \qquad (\mu\varepsilon)$$

$$\varepsilon_{cc} = 1300 + 12.5 f_c \qquad (\mu\varepsilon)$$

$$q = \frac{\xi^{0.745}}{2 + \xi}$$

$$\beta = (2.36 \times 10^{-5})^{[0.25 + (\xi - 0.5)^7]} f_c^2 \times 3.51 \times 10^{-4}$$

$$\xi = \frac{f_y A_s}{f_{ck} A_c}$$

Where f_c denotes the concrete cylinder axial compressive strength (MPa).

3. Parameters selection of FEM model and validation with experimental results

3.1 Element types selection

Eight-node hexahedral finite element named SOLID65 in ANSYS is selected to simulate the elements of concrete in CFST, which can take into account numerous nonlinear behaviors of concrete material, such as concrete cracking in three orthogonal directions, crushing, plastic deformation and creep, etc. SOLID45 is chosen for steel tube and steel plate (e.g., Choi 2010) . As for the simulation of interaction between the steel and concrete, perfect bond is assumed and it is reasonable in numerical analysis of simple CFST models (e.g., Sundarraja 2011, Amr 2007, JIANG 2000). In addition, it will be certificated by the following calculations.

3.2 Parameter selection and validation

According to the experimental data of a set of vertically compressed CFST members, the dimension of steel tube is Φ108×4 mm with two different length. The yield strength of steel tube is 338.9 Mpa, the Young's modulus is 2.01×10^5 Mpa and Poisson's ratio is 0.3. The cubic compressive strength of concrete is 35.7 Mpa and the Young's modulus is 3.15×10^4 Mpa and Poisson's ratio is 0.2. Bilinear Kinematic Hardening Plasticity Model (BKIN) and Mises Yield Criterion is used for steel tube, and Multilinear Isotropic Hardening Plasticity Model (CONC+MISO) in ANSYS is used for concrete. Concrete's shear transfer coefficient of gaping fissure and close crack is 0.35 and 0.9 respectively, and the uniaxial tensile strength is 2.20 Mpa. A semi-rigid cushion is used to eliminate the effect of stress concentration at the loading end.

Verification model with length of 324 mm is shown as Fig. 3. For FEM model C-9 (L/D > 6) in Table 1, a forced-deflection of 0.001*L is applied on the free end (loading end) to simulate the imperfection and residual stress of steel pipe approximately, and the direction of forced-deflection is consistent with gravity. This simplified method will be also used in the following analysis to consider the residual stress and initial deflection of CFST members. Details of these two specimens are listed in Table 1.

In Table1, D is the diameter of CFST, t is the thickness of steel tube and L is the length.

As shown in Table 1, the selected element types and parameters and the model meshing are reasonable in FEM simulation.

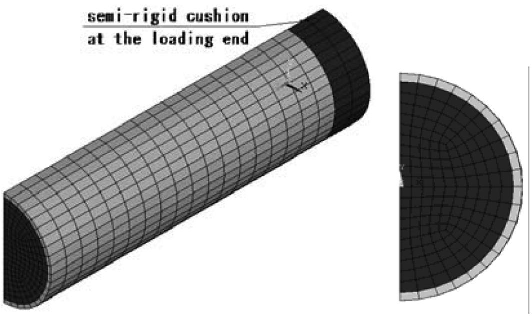

Fig. 3 Verification model

Fig. 4 The finite element model of steel tube of low compress ring (Foshan Century Lotus Stadium)

Table 1 Compressive bear capacity of CFST members from results of test and FEM calculation

Test number	Dimension of steel tube (mm) D×t×L	Experimental value (e.g., Cai 2007) N_u (kN)	FEM value N_l (kN)
C-3	108×4×324	1073	1075.2
C-9	108×4×1080	837	844.8

4. FEM analysis of full-size CFST members

4.1 Gravity effect of horizontal casting CFST member before concrete hardening

The dimension of steel tube of lower compress ring of Foshan Century Lotus Stadium is Φ1200 mm ×22 mm×24 m (D×t×L). Both ends of this member are simply supported, and the model with length of 12 m is used to study its mechanical behavior symmetrically. Fig. 4 shows a symmetric model and its FEM meshes.

With consideration of the process of concrete casting, concrete can not form the stiffness to bear the deadweight itself immediately after casting. At this time, concrete could be regarded as fluid inside steel tube. In order to simulate the behavior of "liquid" concrete, a gradient surface pressure is used to act on the wall of steel tube. The deflection of steel tube is 29.863 mm at the free end, and the maximum MISES stress reaches 99.6 Mpa (no including residual stress). The deflection and MISES stress contours of steel tube at this point are shown in Fig. 5.

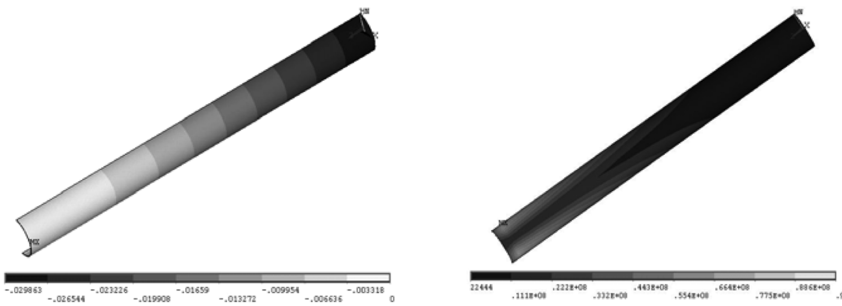

Fig. 5 The vertical deflection contour and MISES stress contour of steel tube with the deadweight of fluid concrete and steel tube

4.2 Calculation of transverse CFST member considering horizontal casting effect (Model 1)

The calculation is achieved through the following steps. First step is “killing” the inside concrete elements and transforming the deadweight of “flowing” concrete to a gradient surface pressure on the internal wall of steel tube. Second step is appending the initial stress and deflection of steel tube which had existed before the hardening of concrete. Third step is restarting and activating (hardening) concrete elements based on the stress and deflection of steel tube in second step. Final step is calculating the bearing capacity under axial load by nonlinear analysis.

The yield strength of steel tube is 345 MPa and the concrete strength is C50. Bilinear Kinematic Hardening Plasticity Model (BKIN) and Mises Yield Criterion are used for steel tube, and Multilinear Isotropic Hardening Plasticity Model (CONC+MISO) in ANSYS is required for concrete. The ultimate compressive bearing capacity and deflection obtained from results of FEM model are 44,928 kN and 100.209 mm respectively. The ultimate deflection and MISES stress of model 1 are shown in Fig. 6.

4.3 Calculation of transverse CFST member regardless of horizontal casting effect (Model 2)

With comparison to model 1, a new FEM model (model 2) is built to simulate another construction procedure in which there are adequate temporary supports along the CFST member during concrete casting and hardening. Because the gravity of CFST member is completely supported by temporary

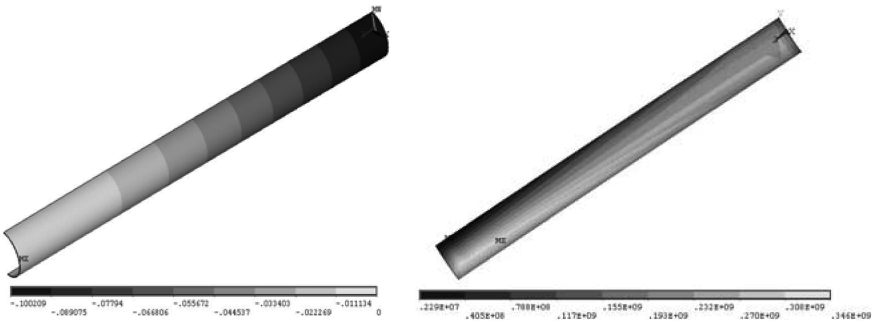

Fig. 6 The ultimate vertical deflection contour and MISES stress contour of steel tube considering horizontal casting effect

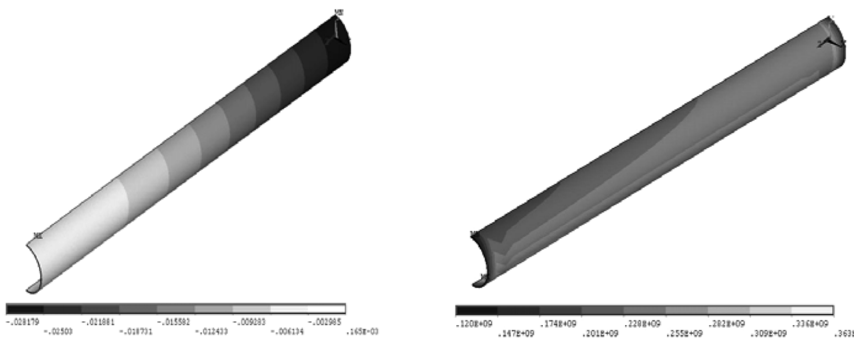

Fig. 7 The ultimate vertical deflection contour and MISES stress contour of steel tube regardless of horizontal casting effect

Table 2 Bearing capacities and deflections based on different construction processes

Members	Model 1	Model 2
Ultimate compressive bearing capacity	44,928 (kN)	54,144 (kN)
Ultimate deflection	100.209 (mm)	28.179 (mm)

supports, there will be no initial stress and deflection produced by gravity in CFST member at first. So concrete horizontal casting effect could be neglected in this model and only the residual stress and initial deflection of CFST members should be considered.

In FEM calculation, all elements in model 2 are activated at the same time. The ultimate compressive bearing capacity and deflection obtained from results of FEM model are 54,144 kN and 28.179 mm respectively. The ultimate deflection and MISES stress of model 2 are shown in Fig. 7.

The ultimate compressive bearing capacities and deflections of these two models are listed in Table 2.

Table 2 shows that the difference of the ultimate compressive bearing capacity of CFST members between model 1 and model 2 reaches for 17.02%, while the difference of ultimate deflection is 255.62%. The failure modes of these two models are both compression-flexure failure, which are produced by the yielding of partial elements in the middle span of simply-supported CFST members.

5. The influence of slenderness ratio (*L/D*) and confining parameter (*D/t*)

In order to study the influence of slenderness ratio and confining parameter on the behavior of CFST member, a set of CFST models of horizontally cast CFST members based on different construction processes are calculated and all results are listed in Table 3.

D is the diameter of CFST. t is the thickness of steel tube. L is the length of CFST. P_1 is the ultimate bearing capacity regardless of construction process, which is almost the same as the bearing capacity of vertically placed CFST, P_2 is the ultimate bearing capacity considering construction process, and δ is the difference radio between P_1 and P_2, where

$$\delta = \frac{P_1 - P_2}{P_1} \times 100\%$$

Table 3.1 The ultimate bearing capacity with $D/t = 20$

CFST members no.	Diameter D (mm)	D/t	L/D	P_1 (kN)	P_2 (kN)	Difference radio δ
C50_D/t20_3000	1000	20	3	110592	110592	0
C50_D/t20_7000	1000	20	7	87552	87552	0
C50_D/t20_11000	1000	20	11	78336	78336	0
C50_D/t20_15000	1000	20	15	76032	74880	0.01515
C50_D/t20_19000	1000	20	19	72576	67968	0.06349
C50_D/t20_23000	1000	20	23	64512	55296	0.14286
C50_D/t20_27000	1000	20	27	50688	42624	0.15909
C50_D/t20_31000	1000	20	31	39168	32256	0.17647
C50_D/t20_35000	1000	20	35	31104	24192	0.22222

Table 3.2 The ultimate bearing capacity with $D/t = 25$

CFST members no.	Diameter D (mm)	D/t	L/D	P_1 (kN)	P_2 (kN)	Difference radio δ
C50_D/t25_3000	1000	25	3	86400	86400	0
C50_D/t25_7000	1000	25	7	77184	77184	0
C50_D/t25_11000	1000	25	11	70272	70272	0
C50_D/t25_15000	1000	25	15	65664	64512	0.01754
C50_D/t25_19000	1000	25	19	63360	58752	0.07273
C50_D/t25_23000	1000	25	23	56448	47232	0.16327
C50_D/t25_27000	1000	25	27	43776	35712	0.18421
C50_D/t25_31000	1000	25	31	33024	26880	0.18605
C50_D/t25_35000	1000	25	35	27648	19968	0.27778

Table 3.3 The ultimate bearing capacity with $D/t = 30$

CFST members no.	Diameter D (mm)	D/t	L/D	P_1 (kN)	P_2 (kN)	Difference radio δ
C50_D/t30_3000	1000	30	3	74880	74880	0
C50_D/t30_7000	1000	30	7	70272	70272	0
C50_D/t30_11000	1000	30	11	63360	63360	0
C50_D/t30_15000	1000	30	15	59904	58752	0.01923
C50_D/t30_19000	1000	30	19	56448	51840	0.08163
C50_D/t30_23000	1000	30	23	50688	41472	0.18182
C50_D/t30_27000	1000	30	27	39168	31104	0.20588
C50_D/t30_31000	1000	30	31	29552	23040	0.22036
C50_D/t30_35000	1000	30	35	23808	16896	0.29032

Table 3.4 The ultimate bearing capacity with $D/t = 35$

CFST members no.	Diameter D (mm)	D/t	L/D	P_1 (kN)	P_2 (kN)	Difference radio δ
C50_D/t35_3000	1000	35	3	67968	67968	0
C50_D/t35_7000	1000	35	7	64512	64512	0
C50_D/t35_11000	1000	35	11	58752	58752	0
C50_D/t35_15000	1000	35	15	56448	52992	0.06122
C50_D/t35_19000	1000	35	19	52992	47232	0.1087
C50_D/t35_23000	1000	35	23	43008	36864	0.14286
C50_D/t35_27000	1000	35	27	34560	27648	0.2000
C50_D/t35_31000	1000	35	31	26880	19968	0.25714
C50_D/t35_35000	1000	35	35	20736	14976	0.27778

Table 3.5 The ultimate bearing capacity with $D/t = 40$

CFST members no.	Diameter D (mm)	D/t	L/D	P_1 (kN)	P_2 (kN)	Difference radio δ
C50_D/t40_3000	1000	40	3	64512	64512	0
C50_D/t40_7000	1000	40	7	59904	59904	0
C50_D/t40_11000	1000	40	11	55296	55296	0
C50_D/t40_15000	1000	40	15	50688	49536	0.02273
C50_D/t40_19000	1000	40	19	48384	42624	0.11905
C50_D/t40_23000	1000	40	23	42624	33408	0.21622
C50_D/t40_27000	1000	40	27	31488	24576	0.21951
C50_D/t40_31000	1000	40	31	24192	17856	0.2619
C50_D/t40_35000	1000	40	35	19008	13248	0.30303

Table 3.6 The ultimate bearing capacity with $D/t = 45$

CFST members no.	Diameter D (mm)	D/t	L/D	P_1 (kN)	P_2 (kN)	Difference radio δ
C50_D/t45_3000	1000	45	3	59904	59904	0
C50_D/t45_7000	1000	45	7	57600	57600	0
C50_D/t45_11000	1000	45	11	51840	51840	0
C50_D/t45_15000	1000	45	15	48384	46080	0.04762
C50_D/t45_19000	1000	45	19	46080	40320	0.12500
C50_D/t45_23000	1000	45	23	40320	31104	0.22857
C50_D/t45_27000	1000	45	27	29952	23040	0.23077
C50_D/t45_31000	1000	45	31	23040	16128	0.3000
C50_D/t45_35000	1000	45	35	17856	11520	0.35484

Table 3.7 The ultimate bearing capacity with $D/t = 50$

CFST members no.	Diameter D (mm)	D/t	L/D	P_1 (kN)	P_2 (kN)	Difference radio δ
C50_D/t50_3000	1000	50	3	57600	57600	0
C50_D/t50_7000	1000	50	7	55296	55296	0
C50_D/t50_11000	1000	50	11	49536	49536	0
C50_D/t50_15000	1000	50	15	46080	43776	0.05000
C50_D/t50_19000	1000	50	19	43776	36864	0.15789
C50_D/t50_23000	1000	50	23	35328	28416	0.19565
C50_D/t50_27000	1000	50	27	27648	20736	0.25000
C50_D/t50_31000	1000	50	31	21312	14976	0.2973
C50_D/t50_35000	1000	50	35	16704	10368	0.37931

Table 3.8 The ultimate bearing capacity with $D/t = 55$

CFST members no.	Diameter D (mm)	D/t	L/D	P_1 (kN)	P_2 (kN)	Difference radio δ
C50_D/t55_3000	1000	55	3	55296	55296	0
C50_D/t55_7000	1000	55	7	52992	52992	0
C50_D/t55_11000	1000	55	11	47232	47232	0
C50_D/t55_15000	1000	55	15	43776	42624	0.02632
C50_D/t55_19000	1000	55	19	41472	35712	0.13889
C50_D/t55_23000	1000	55	23	33792	26880	0.20455
C50_D/t55_27000	1000	55	27	26880	19200	0.28571
C50_D/t55_31000	1000	55	31	20736	13824	0.33333
C50_D/t55_35000	1000	55	35	16128	9216	0.42857

Table 3.9 The ultimate bearing capacity with $D/t = 60$

CFST members no.	Diameter D (mm)	D/t	L/D	P_1 (kN)	P_2 (kN)	Difference radio δ
C50_D/t60_3000	1000	60	3	52992	52992	0
C50_D/t60_7000	1000	60	7	50668	50668	0
C50_D/t60_11000	1000	60	11	46080	46080	0
C50_D/t60_15000	1000	60	15	42624	40320	0.05405
C50_D/t60_19000	1000	60	19	40320	33408	0.17143
C50_D/t60_23000	1000	60	23	32256	25344	0.21429
C50_D/t60_27000	1000	60	27	25344	18432	0.27273
C50_D/t60_31000	1000	60	31	19584	12672	0.35294
C50_D/t60_35000	1000	60	35	14592	8448	0.42105

Table 3.10 The ultimate bearing capacity with $D/t = 65$

CFST members no.	Diameter D (mm)	D/t	L/D	P_1 (kN)	P_2 (kN)	Difference radio δ
C50_D/t65_3000	1000	65	3	52992	52992	0
C50_D/t65_7000	1000	65	7	49536	49536	0
C50_D/t65_11000	1000	65	11	44928	44928	0
C50_D/t65_15000	1000	65	15	41472	39168	0.05556
C50_D/t65_19000	1000	65	19	39168	32256	0.17647
C50_D/t65_23000	1000	65	23	31488	24576	0.21951
C50_D/t65_27000	1000	65	27	24576	16896	0.3125
C50_D/t65_31000	1000	65	31	19584	11520	0.41176
C50_D/t65_35000	1000	65	35	13824	7680	0.44444

Table 3.11 The ultimate bearing capacity with $D/t = 70$

CFST members no.	Diameter D (mm)	D/t	L/D	P_1 (kN)	P_2 (kN)	Difference radio δ
C50_D/t70_3000	1000	70	3	50688	50688	0
C50_D/t70_7000	1000	70	7	48384	48384	0
C50_D/t70_11000	1000	70	11	44928	44928	0
C50_D/t70_15000	1000	70	15	40320	38016	0.05714
C50_D/t70_19000	1000	70	19	38016	31104	0.18182
C50_D/t70_23000	1000	70	23	29952	23040	0.23077
C50_D/t70_27000	1000	70	27	23808	16896	0.29032
C50_D/t70_31000	1000	70	31	18432	10944	0.40625
C50_D/t70_35000	1000	70	35	13440	6912	0.48571

Table 3.12 The ultimate bearing capacity with $D/t = 75$

CFST members no.	Diameter D (mm)	D/t	L/D	P_1 (kN)	P_2 (kN)	Difference radio δ
C50_D/t75_3000	1000	75	3	48384	48384	0
C50_D/t75_7000	1000	75	7	46080	46080	0
C50_D/t75_11000	1000	75	11	42624	42624	0
C50_D/t75_15000	1000	75	15	39168	36864	0.05882
C50_D/t75_19000	1000	75	19	36480	29760	0.18421
C50_D/t75_23000	1000	75	23	29184	22272	0.23684
C50_D/t75_27000	1000	75	27	22464	15552	0.30769
C50_D/t75_31000	1000	75	31	17856	10368	0.41935
C50_D/t75_35000	1000	75	35	13056	6144	0.52941

Table 3.13 The ultimate bearing capacity with $D/t = 80$

CFST members no.	Diameter D (mm)	D/t	L/D	P_1 (kN)	P_2 (kN)	Difference radio δ
C50_D/t80_3000	1000	80	3	48384	48384	0
C50_D/t80_7000	1000	80	7	47232	47232	0
C50_D/t80_11000	1000	80	11	41472	41472	0
C50_D/t80_15000	1000	80	15	38016	35712	0.06061
C50_D/t80_19000	1000	80	19	35520	28800	0.18919
C50_D/t80_23000	1000	80	23	28416	21540	0.24198
C50_D/t80_27000	1000	80	27	21888	14976	0.31579
C50_D/t80_31000	1000	80	31	17280	9600	0.44444
C50_D/t80_35000	1000	80	35	12672	5529.6	0.56364

Table 3.14 The ultimate bearing capacity with $D/t = 85$

CFST members no.	Diameter D (mm)	D/t	L/D	P_1 (kN)	P_2 (kN)	Difference radio δ
C50_D/t85_3000	1000	85	3	48384	48384	0
C50_D/t85_7000	1000	85	7	44928	44928	0
C50_D/t85_11000	1000	85	11	41472	41472	0
C50_D/t85_15000	1000	85	15	37440	35520	0.05128
C50_D/t85_19000	1000	85	19	34560	27840	0.19444
C50_D/t85_23000	1000	85	23	27648	20736	0.25000
C50_D/t85_27000	1000	85	27	21312	13824	0.35135
C50_D/t85_31000	1000	85	31	16704	8832	0.47126
C50_D/t85_35000	1000	85	35	12288	5068.8	0.58750

It can be seen from Table 3 that P_1 is not less than P_2 at any time. While $L/D \geq 15$, the value of $(P_1\text{-}P_2)$ grows faster than the growth of L/D with same value of D/t. Similarly, when L/D is fixed, P_1 is larger than P_2, and the value of $(P_1\text{-}P_2)$ grows together with the growth of D/t.

In most countries, the design codes only define the calculating method of the bearing capacity regardless of construction process (P_1). In order to consider the concrete horizontal casting effect on bearing capacity of CFST, the most convenient way is to define a dimensionless reduction coefficient φ_p (where $\varphi_p = P_2/ P_1$). φ_p is associated with L/D and D/t, and it can be defined as Eq. (4)

$$\varphi_p = 1 - \delta(x, y) \tag{4}$$

Least squares theory is used to perform the surface fitting about the Fig. 8 with Matlab. The formula can be written as Eq. (5)

$$\delta(x, y) = a_0 + a_1 x + a_2 y + a_3 xy + a_4 x^2 + a_5 y^2 \tag{5}$$

The coefficient equation can be written as Eq. (6) with Least squares theory.

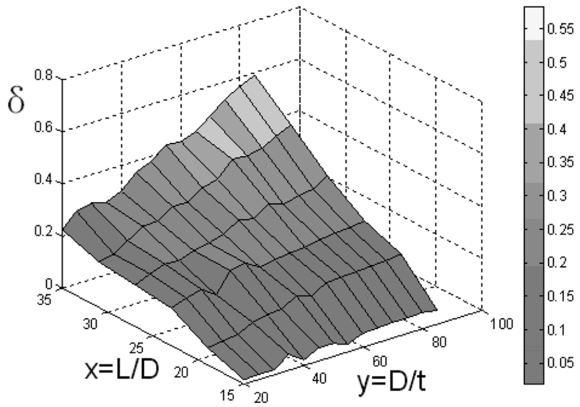

Fig. 8 The folding surface contour of δ

$$\begin{bmatrix} 84 & \Sigma x_i & \Sigma y_i & \Sigma x_i y_i & \Sigma x_i^2 & \Sigma y_i^2 \\ \Sigma x_i & \Sigma x_i^2 & \Sigma x_i y_i & \Sigma x_i^2 y_i & \Sigma x_i^3 & \Sigma x_i y_i^2 \\ \Sigma y_i & \Sigma x_i y_i & \Sigma y_i^2 & \Sigma x_i y_i^2 & \Sigma x_i^2 y_i & \Sigma y_i^3 \\ \Sigma x_i y_i & \Sigma x_i^2 y_i & \Sigma x_i y_i^2 & \Sigma x_i^2 y_i^2 & \Sigma x_i^3 y_i & \Sigma x_i y_i^3 \\ \Sigma x_i^2 & \Sigma x_i^3 & \Sigma x_i^2 y_i & \Sigma x_i^3 y_i & \Sigma x_i^4 & \Sigma x_i^2 y_i^2 \\ \Sigma y_i^2 & \Sigma x_i y_i^2 & \Sigma y_i^3 & \Sigma x_i y_i^3 & \Sigma x_i^2 y_i^2 & \Sigma y_i^4 \end{bmatrix} \begin{bmatrix} a_0 \\ a_1 \\ a_2 \\ a_3 \\ a_4 \\ a_5 \end{bmatrix} = \begin{bmatrix} \Sigma z_i \\ \Sigma x_i z_i \\ \Sigma y_i z_i \\ \Sigma x_i y_i z_i \\ \Sigma x_i^2 z_i \\ \Sigma y_i^2 z_i \end{bmatrix} \tag{6}$$

Coefficients a_0, a_1, a_2, a_3, a_4, a_5 can be solved immediately by Matlab and the fitting surface can be drawn as Fig. 9. The fitting surface is written as Eq. (7).

$$\begin{aligned} \delta(x, y) &= -0.11983763996436 - 0.00245795980522x + 0.01066427877536y \\ &+0.00023477375498xy - 0.00000553007224x^2 - 0.00012021681146y^2 \end{aligned} \tag{7}$$

6. Calculation of coefficient φ_p

According to Eq. (7) and Fig. 9, when $L/D \geq 15$, φ_p can be defined as Eqs. (8) and (9).

$$\begin{aligned} 1 - \varphi_p &= -0.11983764 - 0.00245796\left(\frac{L}{D}\right) + 0.01066428\left(\frac{D}{t}\right) \\ &+0.00023477\left(\frac{L}{D}\right) \bullet \left(\frac{D}{t}\right) - 0.00000553\left(\frac{L}{D}\right)^2 - 0.0001202\left(\frac{D}{t}\right)^2 \end{aligned} \tag{8}$$

$$\begin{aligned} \varphi_p &= 1.11983764 + 0.00245796\left(\frac{L}{D}\right) - 0.01066428\left(\frac{D}{t}\right) \\ &-0.00023477\left(\frac{L}{D}\right) \bullet \left(\frac{D}{t}\right) + 0.00000553\left(\frac{L}{D}\right)^2 + 0.0001202\left(\frac{D}{t}\right)^2 \end{aligned} \tag{9}$$

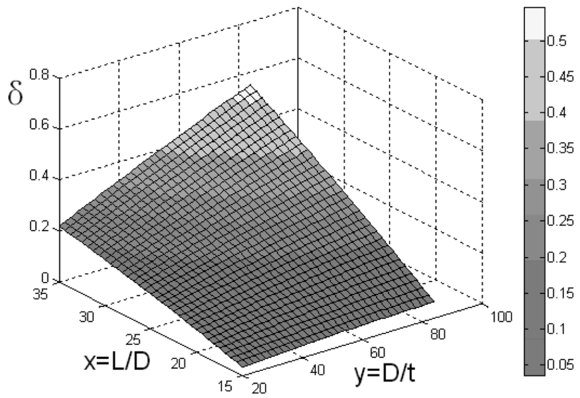

Fig. 9 The fitting smooth surface contour of δ

The samples of φ_p from Table 3 and the corresponding calculation results from the fitting Eq. (9) are compared and checked as following figures (Fig. 10~15).

It can be seen from these figures that the results from fitting equation are relatively close to tested samples in Table 3. It can be expected that both of them will get closer with the increasing of *L*/*D*.

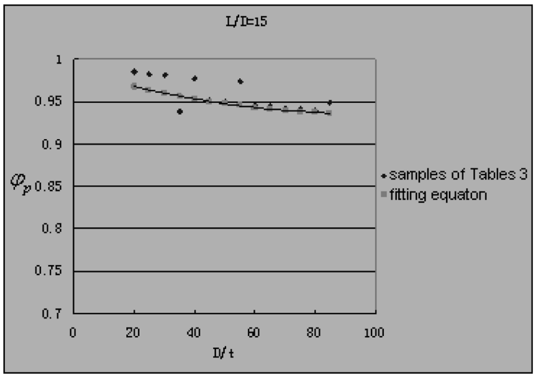

Fig. 10 Comparison of φ_p between samples of Table3 and results of fitting Eq. (9) when *L*/*D* = 15

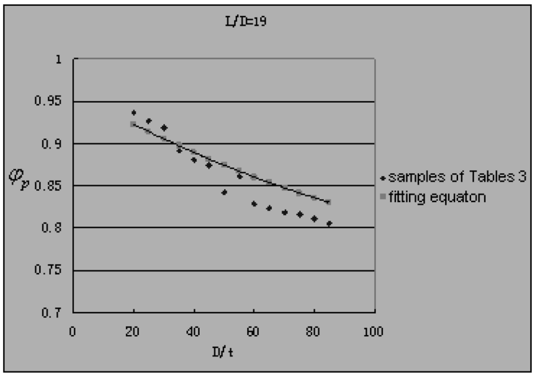

Fig. 11 Comparison of φ_p between samples of Table3 and results of fitting Eq. (9) when *L*/*D* = 19

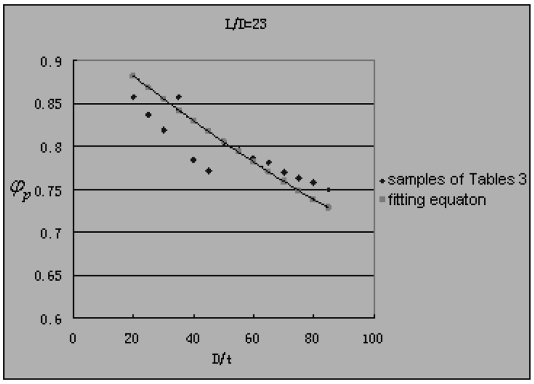

Fig. 12 Comparison of φ_p between samples of Table3 and results of fitting Eq. (9) when *L*/*D* = 23

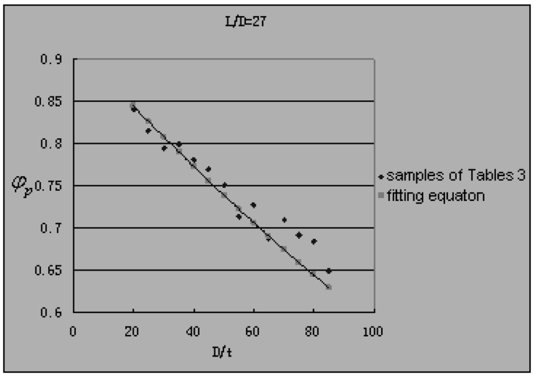

Fig. 13 Comparison of φ_p between samples of Table3 and results of fitting Eq. (9) when $L/D = 27$

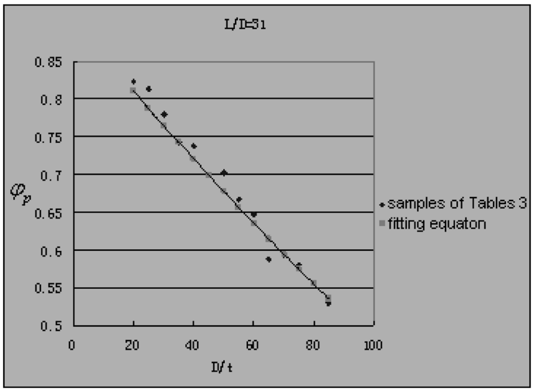

Fig. 14 Comparison of φ_p between samples of Table3 and results of fitting Eq. (9) when $L/D = 31$

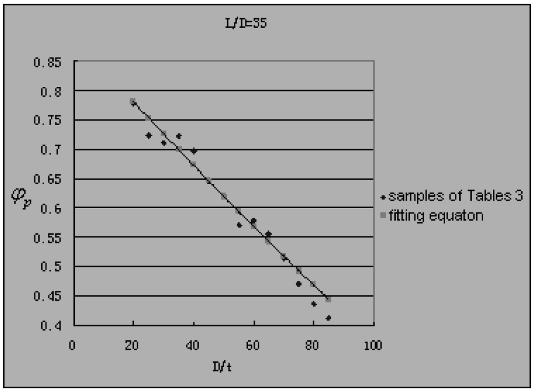

Fig. 15 Comparison of φ_p between samples of Table3 and results of fitting Eq. (9) when $L/D = 35$

7. Conclusions

Based on different construction processes, the ultimate bearing capacity of horizontally cast CFST members is analyzed in this paper. It is shown that different construction processes will produce different bearing capacity of CFST members. Based on other's tests, a series of parameterized finite element models are calculated and the results are integrated into a useful fitting equation by mathematical statistics method.

The bearing capacity of CFST members is associated with slenderness ratio (L/D) and confining parameter (D/t). CFST's ultimate bearing capacity considering concrete horizontal casting effect (P_2) is relatively smaller than that regardless of concrete horizontal casting effect (P_1). A dimensionless reduction coefficient φ_p is defined to describe the difference between P_1 and P_2. As P_1 can be easily calculated on the basis of most design codes, P_2 can also be obtained according to φ_p with different L/D and D/t.

From the results of Table 3, concrete horizontal casting effect can be ignored when L/D is not greater than 15, that means φ_p equals 1.0 when $L/D \leq 15$ and Eq. (9) is significant only when $L/D \geq 15$.

References

ANSYS Element Reference. (1998), Electronic Release [M], SAS IP, INC.

ANSYS Theory Reference. (1998), Electronic Release, SAS IP, Inc.

Attard, M. M. and Setunge, S. (1996), "Stress-strain relationship of confined and unconfined concrete", *ACI Materials Journal*, **93**(5), 432-442.

Choi, K. and Xiao, Y. (2010), "Analytical model of circular CFRP confined concrete-filled steel tubular columns under axial compression", *Journal of Composites for Construction*, **14**(1), 125-133.

Furlong, R. W. (1967), "Strength of steel-encased concrete beam-columns", *J. Struct. Engrg.*, **94**(1), 267-281.

Jiang, L., Zhou, W. and Qi, J. (2011), "Numerical method and experimental study on the ultimate load carrying capacity of four tube CFST latticed columns", *2011 International Conference on Structures and Building Materials*, Guangzhou, China, January.

Han, L. (2007), *Concrete Filled Steel Tubular Structures from Theory to Practice*. Beijing: China Science Press. (in Chinese)

Hatzigeorgiou, G. D. (2008), "Numerical model for the behavior and capacity of circular CFT columns, Part I: Theory", *Eng. Struct.*, **30**(6), 1573-1578.

Knowles, R. B., and Park, R. (1969). "Strength of concrete filled steel tubular columns", *J. Struct. Engrg.*, **95**(12), 2565-2587.

Lee, J. and Fenves, G. L. (1998), "Plastic-damage model for cyclic loading of concrete structures". *J. Eng. Mech.*, **124**(8), 892-900.

Lu, H., Han, L. and Zhao, X. (2009), "Analytical behavior of circular concrete-filled thin-walled steel tubes subjected to bending", *Thin-Walled Structures*, **47**(3), 346-358.

Lubliner, J., Oliver, J., Oller, S. and Onate, E. (1989), "A plastic-damage model for concrete", *International Journal of Solids and Structures,* **25**(3), 229-326.

Luo, H., Yan, Z. G. and An, M. Z. (2011), "Finite element analysis of RPC-filled steel tube stub columns", *2nd International Conference on Manufacturing Science and Engineering*, Guilin, China, April.

Masmoudi, R., et al. (2010), "Experimental investigation on the behaviour of concrete-filled FRP tubes under flexural load", *Annual Conference of the Canadian Society for Civil Engineering 2010*, Winnipeg, MB, Canada, June.

Mohamed, H. M. and Masmoudi, R. (2010), "Flexural strength and behavior of steel and FRP-reinforced concrete-filled FRP tube beams", *Eng. Struct.*, **32**(11), 3789-3800.

Probst, A. D., et al. (2010), "Composite flexural behavior of full-scale concrete-filled tubes without axial loads", *J. Struct. Eng.*, **136**(11), 1401-1412.

Schneider, S. P. (1998), "Axially Loaded Concrete-Filled Steel Tubes," *J. Struct. Eng.*, **124** (10), 1125-1138

Sun, G. *et al.* (2009), "Simulation calculation research of long span CFST arch bridge based on optimization algorithm", *2009 2nd International Conference on Intelligent Computing Technology and Automation*,

Changsha, Hunan, China, October.
Valipour, H. R. and Foster, S. J. (2010), "Nonlinear static and cyclic analysis of concrete-filled steel columns", *J. Constr. Steel Res.*, **66**(6), 793-802.
Yang, Y. and Han, L. (2011), "Behaviour of concrete filled steel tubular (CFST) stub columns under eccentric partial compression", *Thin-Walled Structures*, **49**(2), 379-395.
Zha Xiaoxiong and ZHONG Shantong (1997), "The behavior effect on concrete filled steel tubular members subjected to compression under the initial stress of steel tube based on the finite element method", *Journal of Harbin University of Civil Engineering and Architecture.* (in Chinese)
Sundarraja, M. C. and GaneshPrabhu, G. (2011), "Finite element modelling of CFRP jacketed CFST members under flexural loading", *Thin-Walled Structures*, **49**, 1483-1491.
Shaat Amr and Fam Amir (2007), "Finite element analysis of slender HSS columns strengthened with high modulus composites". *Steel. Compos. Struct.*, **7**, 19-34.
JIANG Shao-fei, HAN Lin-hai and QIAO Jing-chuan. (2000), "Initial discussion on the bond problems of steel and concrete in Concrete Filled Steel Tubes (CFST)", *Journal of Harbin University of C. E. & Architecture*, **33**(2), 24-28. (in Chinese)

CC